AIP Applied Physics Letters

Enhanced power factor and reduced thermal conductivity of a half-Heusler derivative Ti9Ni7Sn8: A bulk nanocomposite thermoelectric material

D. K. Misra, A. Rajput, A. Bhardwaj, N. S. Chauhan, and Sanjay Singh

Citation: Applied Physics Letters **106**, 103901 (2015); doi: 10.1063/1.4914504
View online: http://dx.doi.org/10.1063/1.4914504
View Table of Contents: http://scitation.aip.org/content/aip/journal/apl/106/10?ver=pdfcov
Published by the AIP Publishing

Articles you may be interested in
Improvement of thermoelectric properties for half-Heusler TiNiSn by interstitial Ni defects
J. Appl. Phys. **110**, 063710 (2011); 10.1063/1.3633518

Thermoelectric performance of half-Heusler compounds TiNiSn and TiCoSb
J. Appl. Phys. **105**, 013709 (2009); 10.1063/1.3056384

Effect of Ti substitution on the thermoelectric properties of (Zr,Hf)NiSn half-Heusler compounds
Appl. Phys. Lett. **86**, 082105 (2005); 10.1063/1.1868063

Grain structure effects on the lattice thermal conductivity of Ti-based half-Heusler alloys
Appl. Phys. Lett. **81**, 43 (2002); 10.1063/1.1488698

Effects of partial substitution of Ni by Pd on the thermoelectric properties of ZrNiSn-based half-Heusler compounds
Appl. Phys. Lett. **79**, 4165 (2001); 10.1063/1.1425459

This article is copyrighted as indicated in the article. Reuse of AIP content is subject to the terms at: http://scitation.aip.org/termsconditions. Downloaded to IP: 14.139.60.97 On: Tue, 20 Oct 2015 09:55:02

Enhanced power factor and reduced thermal conductivity of a half-Heusler derivative $Ti_9Ni_7Sn_8$: A bulk nanocomposite thermoelectric material

D. K. Misra,[1,a)] A. Rajput,[1] A. Bhardwaj,[1] N. S. Chauhan,[1] and Sanjay Singh[2]
[1]*CSIR Network of Institutes for Solar Energy, Division of Materials Physics and Engineering, CSIR National Physical Laboratory, Dr. Krishnan Marg, New Delhi 110012, India*
[2]*Max Planck Institute for Chemical Physics of Solids, Nöthnitzer Strasse 40, D-01187 Dresden, Germany*

(Received 26 December 2014; accepted 22 February 2015; published online 11 March 2015)

We report a half-Heusler (HH) derivative $Ti_9Ni_7Sn_8$ with VEC = 17.25 to investigate the structural changes for the optimization of high thermoelectric performance. The structural analysis reveals that the resulting material is a nanocomposite of HH and full-Heusler with traces of Ti_6Sn_5 type-phase. Interestingly, present nanocomposite exhibits a significant decrease in thermal conductivity due to phonon scattering and improvement in the power factor due to combined effect of nanoinclusion-induced electron injection and electron scattering at interfaces, leading to a boost in the ZT value to 0.32 at 773 K, which is 60% higher than its bulk counterpart HH TiNiSn. © *2015 AIP Publishing LLC*. [http://dx.doi.org/10.1063/1.4914504]

The half-Heusler (HH) materials with varying valence electron concentration per unit cell (VEC) results to a large number of structures and substructures that can be exploited to enhance the thermoelectric performance.[1–3] The HH materials which exhibit face centered cubic crystal structure [F-4 3m (no. 216)] possess a VEC of 18.[3] With this VEC = 18, variety of behaviors such as semiconductors, semimetals, ferromagnetism, half-metallic ferromagnetism, or anti-ferromagnetism Pauli metals, can exist in series of compounds.[4–6] On the whole, it has also been noticed that such a variety of behaviors may come from the presence of an energy gap in the density of states for the VEC = 18.[7] The HH materials with VEC = 18 has been considered as a potential semiconducting thermoelectric materials. These materials have a decent Seebeck coefficient with moderate electrical conductivity due to combined feature of a narrow energy gap and a slight shift of Fermi level above the top of the valence band.[8] Reports show that both n-type[9–12] and p-type[13–16] with exceptionally large power factor can exist in such compounds and hence may help in making a compatible module for thermoelectric devices. Despite all these favorable properties, the main drawback in this class of thermoelectric materials is the very large thermal conductivity in comparison to other state-of-the-art TE materials[17–22] which hinders to yielding a descent thermoelectric figure of merit, $ZT = \frac{\alpha^2 \sigma T}{\kappa}$, where σ is the electrical conductivity, α is the Seebeck coefficient, κ is the total thermal conductivity, and T is the absolute temperature. These three physical parameters α, σ, and κ are interrelated in such a way that modification to any of these adversely affects the other and hence limits the overall enhancement in ZT.[23]

In the recent years, several strategies such as doping,[9,15] solid solution alloying,[12–14] and nanostructuring[10,16] in HH compound have been adopted to disrupt heat carrying phonons to significantly reduce their κ. Recently, full-Heusler (FH) inclusions within the p and n type HH compounds have been produced by several groups[24–30] by adding excess Co-concentration in p-type MCoSb (where M = Ti, Zr, Hf) and Ni-concentration in n-type MNiSn (where M = Ti, Zr, Hf). A significant decrease in thermal conductivities of these materials was noted.

Most of the half-Heusler with VEC $\approx$ 18 are stable in cubic phase and are potential thermoelectric materials.[3] We believe that exploring the materials with varying VEC and hence modifying the microstructure and electronic structure may also provide a viable path for optimizing high ZT for thermoelectric applications. Herein, an undoped HH derivative with generic composition $Ti_9Ni_7Sn_8$ with VEC = 17.25 per formula unit which is smaller than VEC of 18 for normal TiNiSn HH has been synthesized in order to obtain any structural modifications such as either super cell structure formation of HH if possible similar to a report on $Ru_9Zn_7Sb_8$[2] or otherwise a composite phase material if phase segregation occurs for the improvement in thermoelectric performance.[1,2,31] We observed that despite to the formation of supercell of HH structure, the material exhibits a composite phase consisting of primarily HH and FH with trace amount of Ti_6Sn_5-type phase. Thus, this mismatch in VEC number does not allow this composition to be electronically stabilized as a supercell of HH; rather it leads to the phase separation resulting in a nanocomposite of HH TiNiSn, FH $TiNi_2Sn$, and Ti_6Sn_5 type phase. Interestingly, a drastic reduction in the lattice thermal conductivity ($\sim$55%) was observed which accounts for improvement in ZT $\approx$ 0.32 at 773 K.

The stoichiometric compositions of TiNiSn and $Ti_9Ni_7Sn_8$ were initially melted in an arc-melt furnace. The melted ingot was annealed at 1173 K for one week and subsequently consolidated, employing spark plasma sintering (SPS) technique. The process yielded 12.7 mm diameter bulk dense pellets. The density of the nanocomposite was obtained from pellets using an equipment (Model: METTLER TOLEDO, ML204/A01) based on Archimedes principle. The measured density of the nanocomposite was observed to be 92.5% of

a)Author to whom correspondence should be addressed. Electronic addresses: misradk@nplindia.org and dakkmisra@gmail.com

0003-6951/2015/106(10)/103901/5/$30.00 © 2015 AIP Publishing LLC

This article is copyrighted as indicated in the article. Reuse of AIP content is subject to the terms at: http://scitation.aip.org/termsconditions. Downloaded to IP: 14.139.60.97 On: Tue, 20 Oct 2015 09:55:02

the theoretical density calculated by Reitveld analysis. In present study, TiNiSn is designated as normal bulk HH and $Ti_9Ni_7Sn_8$ HH/(FH, Ti_6Sn_5) is named as bulk nanocomposite.

In order to study the thermoelectric properties, polished bars of about $3 \times 2 \times 10$ mm and disk of 12.7 mm in diameter and 2 mm in thickness were prepared. The Seebeck coefficient and electrical conductivity were measured on bar samples by using commercial equipments (ULVAC, ZEM-3) and thermal diffusivity was measured on disk sample employing laser flash system (Lineseis, LFA 1000). The specific heat capacity was determined using a differential scanning calorimeter (DSC 822^e Metter Toledo). The thermal conductivity calculated as the product of the thermal diffusivity, specific heat capacity, and volume density of the samples. To confirm the reproducibility of sample preparation procedure and reliability of the thermoelectric measurements of normal bulk HH and HH/(FH, Ti_6Sn_5) nanocomposite material, the sample synthesis and thermoelectric properties measurements were repeated three times and values were found to be consistent.

The XRD pattern of SPSed samples of bulk HH TiNiSn and bulk nanocomposite $Ti_9Ni_7Sn_8$ are presented in Figure 1. The XRD peaks of TiNiSn were found to be matching well with those of half-Heusler (Fig. 1(a)), while the XRD pattern of $Ti_9Ni_7Sn_8$ (Fig. 1(b)) indicates the presence of peaks corresponding to HH and FH with traces of Ti_6Sn_5 phase. The Rietveld fitting for the $Ti_9Ni_7Sn_8$ composite is shown in Fig. 1(c). The Rietveld analysis revealed the material to be composite with $97.1 \pm 1.2\%$ in its HH phase, $2.6 \pm 0.2\%$ in FH and traces of metallic Ti_6Sn_5 phase. The detail results of Rietveld refinement are summarized in Table I. Interestingly, the larger width of the XRD peaks compared to the peak width of standard XRD pattern were also noticed indicating the presence of strain in the sample. A strain of 0.58% was estimated by using Williamson-Hall analysis.

In order to examine the finer microstructural details of the bulk nanocomposite $Ti_9Ni_7Sn_8$ material, its transmission electron microscopy (TEM) images are presented in Fig. 2. A low magnification TEM image, Fig. 2(a), reveals a clear phase contrast of TiNiSn-HH (region A) and $TiNi_2Sn$-FH (dotted circle) with traces of Ti_6Sn_5 (region B). The selected area electron diffraction (SAED) pattern, Fig. 2(b), taken from region A confirms the grain to be a single crystalline HH phase with zone axis $[1\bar{1}2]$. An enlarged view of the dotted region [Fig. 2(a)] is presented in Fig. 2(c), showing two phase interface. The Fast Fourier Transform (FFT) taken from a region marked as rectangle in Fig. 2(c) is shown in the inset of Fig. 2(c) which confirms the marked region to be FH phase along $[1\bar{1}2]$ direction parallel to the electron beam. Interestingly, the energy dispersive X-ray spectroscopic (EDS) data obtained from the grains of FH also present the chemical composition to be very close to the FH phase. Fig. 2(e) shows SAED pattern taken from the grain marked as dotted area B revealing a ring pattern which corresponds to the HH phase and additional spot corresponding to Ti_6Sn_5 phase confirming that the white contrast in dotted area B [Fig. 2(a)] is nano precipitates of Ti_6Sn_5 phase. The phases observed in TEM were consistent with the XRD result and also with scanning electron microscopy (SEM) investigation given in the supplementary material (Fig. S1).[41]

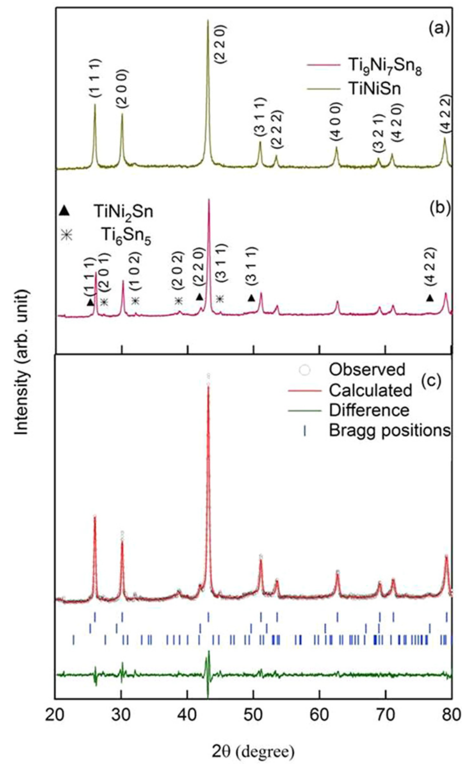

FIG. 1. X-ray diffraction patterns of (a) TiNiSn HH, (b) $Ti_9Ni_7Sn_8$ HH derivative, and (c) Rietveld refinement of $Ti_9Ni_7Sn_8$ showing a composite phase materials. The difference curve is shown in bottom as green solid line. Vertical ticks are Bragg peak positions out of which the upper ticks (blue) correspond to the HH, middle ticks (red) for FH, and lower ticks (black) are for Ti_6Sn_5 phase.

It is worth mentioning that the compositional optimization in HH TiNiSn usually results in a miscibility gap in liquid, allowing a phase separation at the nano-scale, which has been well documented by several groups.[1,32,33] At high temperature, the liquid melt of $Ti_9Ni_7Sn_8$ undergoes solidification at low temperature and crystallizes to form a single solid solution of HH, FH, and Ti_6Sn_5 phases. During cooling, this solid solution further decomposes into stable mixture consisting of HH, FH, and Ti_6Sn_5 phases at room temperature with FH and HH being dominant phases, similar to the observation of Chai and Kimura.[32] It is worth mentioning here that the phase diagram of TiNiSn also suggests that phase separation could occur in alloys with compositions lying between FH and HH, as experimentally observed in the present case. For the present composition of $Ti_9Ni_7Sn_8$, local segregation occurs in such a way that the effective composition lies between HH and FH. The excess amount of Ti, Ni, and Sn might get partly stabilized as Ti_6Sn_5 with finite but small dissolution of Ni in the precipitates of Ti_6Sn_5. The exact mechanism of phase separation through decomposition in $Ti_9Ni_7Sn_8$ is not clear and requires a detailed investigation.

The thermal and electronic transport measurements were carried out to understand the impact of such *in-situ* fabricated multi-phase material on thermoelectric properties. In Fig. 3, we have displayed the temperature dependence of the thermoelectric parameters of the normal HH TiNiSn and bulk nanocomposite $Ti_9Ni_7Sn_8$. The temperature dependent electrical conductivity σ (T) of TiNiSn HH reveals semiconducting

This article is copyrighted as indicated in the article. Reuse of AIP content is subject to the terms at: http://scitation.aip.org/termsconditions. Downloaded to IP: 14.139.60.97 On: Tue, 20 Oct 2015 09:55:02

TABLE I. Detail of Rietveld analysis of the phases present in bulk nanocomposites $Ti_9Ni_7Sn_8$ samples.

Phase 1: TiNiSn half Heusler					Phase 2: $TiNi_2Sn$ full Heusler				
Space group: F-43m					Space group: F m-3m				
Cell (Å): a = 5.9202(3)					Cell (Å): a = 6.0840(16)				
Phase fraction: 97.1(1)%, density: 7.21056 g/cm^3					Phase fraction: 2.62(0.19)%, density: 8.37506 g/cm^3				
Overall temperature factor: 0.55355					Overall temperature factor: 0.59933				
ETA (p-Voigt): 0.3564					ETA (p-Voigt): 0.3278				
Halfwidth U, V, W: 0.43576, −0.07842, 0.08150					Halfwidth U, V, W: 0.43587, −0.07830, 0.07987				
X parameter: 0.0054, FWHM ($\Delta 2\theta_{min}$): 0.285°					X parameter: 0.0051, FWHM ($\Delta 2\theta_{min}$): 0.282°				
Bragg R-factor: 3.13, RF-factor: 1.67					Bragg R-factor: 10.9, RF-factor: 9.7				
Atom	*X*	*Y*	*Z*	*occ*	Atom	*X*	*Y*	*z*	*occ*
Sn	0.25	0.25	0.25	1	Sn	0	0	0	1
Ti	0.75	0.75	0.75	1	Ti	0.5	0.5	0.5	1
Ni	0	0	0	1	Ni	0.25	0.25	0.25	1
Phase 3: Ti_6Sn_5									
Space group: P63/mmc					Atom	*x*	*y*	*Z*	*occ*
Cell (Å): $a = b = 8.991(5)$, c = 5.769(5)									
Phase fraction: 0.28(3)%, density: 7.24478 g/cm^3					Sn1	0	0	0	1
ETA (p-Voigt): 0.3564					Sn2	0.3333	0.6667	0.25	1
Overall temperature factor: 0.42307					Sn3	0.795	0.59	0.25	1
Halfwidth U, V, W: 0.43587, −0.07830, 0.08162					Ti1	0.5	0	0	1
X parameter:0.017931, FWHM ($\Delta 2\theta_{min}$): 0.287°					Ti2	0.165	0.33	0.25	1
Bragg R-factor: 16.9, RF-factor: 9.5									
Global user-weighted Chi^2 (Bragg contrib.): 3.24									

behavior as it increases monotonically with rising temperature (Fig. 3(a)), while σ (T) of bulk nanocomposite $Ti_9Ni_7Sn_8$ [Fig. 3(a)] remained nearly constant up to 425 K, suggesting a typical semimetallic behavior, but a semiconductor like electronic transport was observed beyond this temperature. Fig. 3(b) displays temperature dependent Seebeck coefficient $\alpha(T)$ of the normal HH TiNiSn and $Ti_9Ni_7Sn_8$ nanocomposite. Interestingly, despite to the increase in σ (T) at room temperature for bulk nanocomposite, an increase in $\alpha(T)$ at room temperature was also observed which is rather unusual. Moreover, $\alpha(T)$ increases with rising temperature up to 550 K irrespective to the usual trend of decreasing σ (T). With increasing temperature beyond 550 K, the $\alpha(T)$ decreases. This decrease in $\alpha(T)$ at high temperature beyond 550 K is attributed due to thermally excited minority charge carriers (holes) similar to the case of several semiconducting materials.[38,39] The detailed mechanism of increased $\alpha(T)$ at room temperature will be discussed in forthcoming part of the manuscript. The stability of the material and consistency of electronic transport have been verified by measuring the $\alpha(T)$ and the σ(T) with the samples which was kept at room temperature for 12 weeks and also with sample annealed at 800 °C for 24 h and the results are presented in the inset of Figs. 3(b) and 3(a), respectively. The temperature dependent $\alpha(T)$ and $\alpha(T)$ were observed to be consistent in values and also in trends, presenting the material to be most stable, reproducible, and robust in nature. The power factor computed is presented in Fig. 3(c) showing only a marginal improvement by 6% in bulk nanocomposite compared to the normal HH counterpart. We do also observe that the value of κ for bulk nanocomposite is also reduced significantly which is about 40% in comparison to that of the normal bulk HH sample as evidenced in Fig. 3(d). The low κ of the bulk nanocomposite sample may be due to enhanced heat carrying phonon scattering by the nanoscale

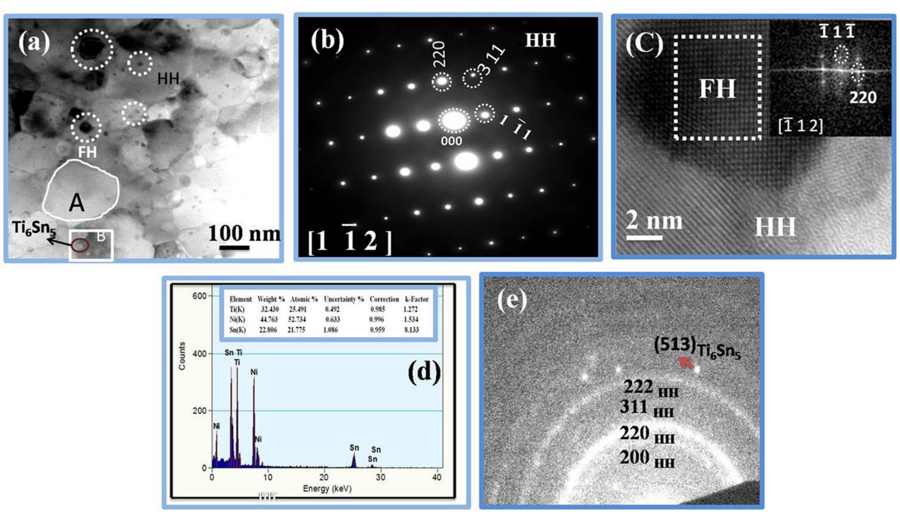

FIG. 2. (a) TEM of $Ti_9Ni_7Sn_8$ showing a composite microstructure of FH (dotted circle), HH (region A), and small impurities of Ti_6Sn_5 (region B). (b) The SAED corresponding to region A confirms single crystalline HH phase with zone axis [$1\bar{1}2$]. (c) HRTEM image from dotted region showing two phase interface. The FFT from a region marked as rectangle (shown in the inset) presents FH phase with zone axis [$1\bar{1}2$]. (d) The EDS data obtained from FH grain indicates composition of FH phase. (e) SAED pattern taken from the grain marked as dotted area B reveals a ring pattern which corresponds to the HH phase and Ti_6Sn_5 phase.

This article is copyrighted as indicated in the article. Reuse of AIP content is subject to the terms at: http://scitation.aip.org/termsconditions. Downloaded to IP: 14.139.60.97 On: Tue, 20 Oct 2015 09:55:02

precipitates of FH and Ti_6Sn_5 and the mesoscale grain boundaries in $Ti_9Ni_7Sn_8$ as can be seen from the microscopic images presented in Fig. 2(a). The lattice thermal conductivity (κ_l) was estimated by subtracting the electronic thermal conductivity (κ_e) from the κ and presented in Fig. 3(e). The κ_e was obtained from Wiedemann-Franz relation. It is observed that the κ_l decreases with increasing temperature displaying 1/T dependence similar to the normal bulk crystalline material.[34,35] The variation in ZT as a function of temperature is shown in Fig. 3(f). A significant enhancement in ZT $\approx$ 0.32 at 773 K was obtained which is about 60% higher than that of bulk TiNiSn HH counterpart. We attribute that this enhancement in ZT is primarily due to drastic reduction in κ.

In order to understand the mechanism of increasing $\alpha(T)$ and $\sigma(T)$ at room temperature simultaneously, Hall coefficient of the samples at 300 K has been measured. These data yield a carrier concentration of $\sim 5.9 \times 10^{19}/\text{cm}^3$ and a mobility of $\sim 73\,\text{cm}^2/\text{V s}$ for normal TiNiSn HH. However, a carrier concentration of $\sim 2.8 \times 10^{19}/\text{cm}^3$ and mobility of $\sim 210\,\text{cm}^2/\text{V s}$ was noted for the bulk nanocomposite $Ti_9Ni_7Sn_8$ indicating a decrease in carrier concentration and increased mobility for bulk nanocomposite.

The observed increase in $\alpha(T)$ of the bulk nanocomposite at room temperature compared to that for bulk normal HH is consistent with its lower carrier density as revealed by Hall measurements. Thus, we believe that observed reduction in carrier density of nanocomposite at room temperature is suggestive of the filtering (trapping) of low energy carrier at energy barrier generated at HH/FH interfaces similar to the other reports which has been verified experimentally and theoretically by several groups.[23,27,36–38] While increased mobility of carriers in the bulk nanocomposite $Ti_9Ni_7Sn_8$ drives the carriers injecting through metallic FH inclusions[24,25] making the material more electrically conducting and hence leads to an increase in electrical conductivity at around 300 K. Thus, the simultaneous increase in the $\sigma(T)$ and $\alpha(T)$ could be attributed to the electron injection phenomenon and scattering of electron at potential barrier generated by HH and FH interfaces. A plausible explanation of this increasing Seebeck coefficient (α) of a composite may also be given in the framework of a model related to the scattering factor and reduced Fermi energy as proposed by Nolas *et al.*[39] where α is expressed as

$$\alpha = \frac{\pi^2}{3}\frac{\kappa_B}{e}\left(r + \frac{2}{3}\right)\left(\frac{1}{\xi}\right), \tag{1}$$

where κ_B is the Boltzmann constant, r is the scattering factor, and ξ is the reduced Fermi energy.

We argue that a significant decrease in the carrier concentration in bulk nanocomposites $Ti_9Ni_7Sn_8$ as observed from the Hall data, reduces the Fermi energy and consequently resulted in an increased Seebeck coefficient.[40] Though mechanism of increased $\alpha(T)$ and $\sigma(T)$ at room temperature has been presented here, however, understanding on the $\alpha(T)$ and $\sigma(T)$ variation with higher temperature requires high temperature Hall measurement which will be the future avenue of this research and needs to be investigated further. Thus, mechanisms for enhancing the electronic properties is primarily interface electron scattering,[23,27,36–38] electron injection through metallic inclusions,[24,25] and direct dependence of Seebeck coefficient on reduced Fermi energy, ξ as suggested by Nolas *et al.*[40]

In conclusion, a generic composition $Ti_9Ni_7Sn_8$ with VEC = 17.25, synthesized by arc melting followed by SPS resulted to an *in-situ* bulk nanocomposite consisting of HH, FH, and a traces of nano-sized Ti_6Sn_5 phase. This microstructural modification derived due to varying VEC in present HH derivative leads to achieve a high ZT $\approx$ 0.32 at 773 K, which is 60% higher as compared to that of the normal bulk TiNiSn HH counterpart. The observed increase in $\alpha(T)$ and $\sigma(T)$ at room temperature is attributed to the electron scattering/filtering and electron injection phenomenon, respectively, while the reduction in thermal conductivity is due to scattering of wide range of heat carrying phonons ranging from nanoscale inclusion of FH and mesoscale grain of HH and also notable mesoscale grain boundaries in $Ti_9Ni_7Sn_8$. Our findings rejuvenates the search for high ZT thermoelectric materials by varying VEC of transition metal based semiconductors in wider family of XYZ (X = Ti, Zr, Hf; Y = Ni, Co; Z = Sn, Sb) with composition $X_{1+x}Y_{1-x}Z$ where significant reduction in thermal conductivity can be optimized. Further controlling the distribution of metallic inclusions by fine tuning the growth parameters through appropriate thermal treatment and with or without doping could be a promising future strategy for enhancing the ZT of several compositions of half-Heusler of XYZ family.

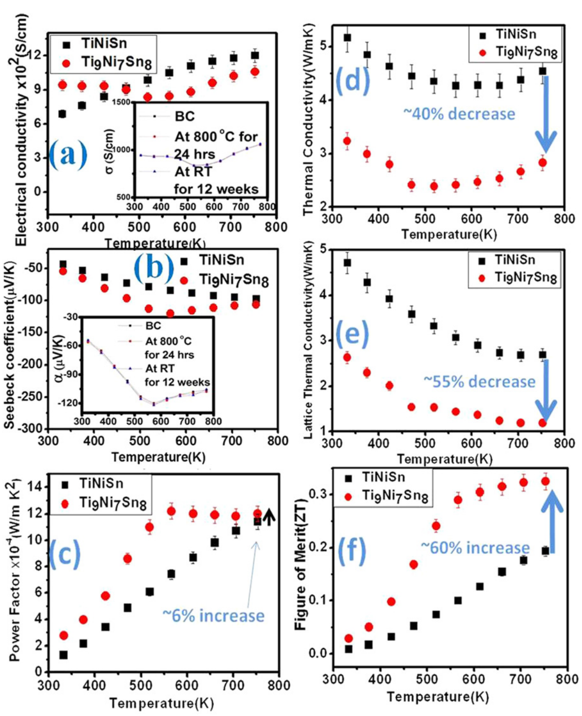

FIG. 3. Temperature dependence of thermoelectric properties of normal bulk HH TiNiSn and bulk nanocomposite $Ti_9Ni_7Sn_8$.

This work was financially supported by CSIR-TAPSUN (CSIR-NWP-54) programme. The authors are graceful to Prof. R. C. Budhani (Ex-Director, CSIR-NPL), for his constant mentoring and support for this project. One of the author S.S. thanks Alexander Von Humboldt Foundation, Germany for fellowship. Dr. Jiji Pullikotil (CSIR-NPL),

This article is copyrighted as indicated in the article. Reuse of AIP content is subject to the terms at: http://scitation.aip.org/termsconditions. Downloaded to IP: 14.139.60.97 On: Tue, 20 Oct 2015 09:55:02

Dr. Vidyanand Singh (CSIR-NPL) are gratefully acknowledged for their useful discussions and comments. The authors A.B., N.S.C., and A.R. acknowledge UGC-CSIR and Research Internship of CSIR-NPL respectively for financial support. The technical support rendered by Mr. Radhey Shyam and Mr. Naval Kishor Upadhyay is gratefully acknowledged.

[1]V. V. Romaka, P. Rogl, L. Romaka, Y. Stadnyk, N. Melnychenko, A. Grytsiv, M. Falmbigl, and N. Skryabina, J. Solid State Chem. **197**, 103 (2013).
[2]D. B. Xiong, Y. Zhao, N. L. Okamoto, C. Pietzonka, T. Waki, and H. Inui, Inorg. Chem. **49**, 10536 (2010).
[3]L. Offernes, P. Ravindran, and A. Kjekshus, J. Alloys Compd. **439**, 37 (2007).
[4]R. A. de Groot, F. M. Mueller, P. G. van Engen, and K. H. J. Buschow, Phys. Rev. Lett. **50**, 2024 (1983).
[5]P. J. Webster and K. R. A. Ziebeck, *Magnetic Properties of Metals and Alloys* (Springer-Verlag, Berlin, 1988).
[6]J. Pierre, R. V. Skolozdra, J. Tobola, S. Kaprzyk, C. Hordequin, M. A. Kouacou, I. Karla, R. Currat, and E. Leliévre-Berna, J. Alloys and Compd. **262–263**, 101 (1997).
[7]J. Tobola, S. Kaprzyk, R. V. Skolozdra, and M. A. Kouacou, J. Phys.: Condens. Matter **10**, 1013 (1998).
[8]F. G. Aliev, V. V. Kozyrkov, R. V. Scolozdra, and K. Durczewski, Z. Phys. B: Condens. Matter **80**, 353 (1990).
[9]S. R. Culp, S. J. Poon, N. Hickman, T. M. Tritt, and J. Blumm, Appl. Phys. Lett. **88**, 042106 (2006).
[10]A. Bhardwaj, D. K. Misra, J. J. Pulikkotil, S. Auluck, A. Dhar, and R. C. Budhani, Appl. Phys. Lett. **101**, 133103 (2012).
[11]A. Bhardwaj and D. K. Misra, J. Mater. Chem. A **2**, 20980 (2014).
[12]S. Sakurada and N. Shutoh, Appl. Phys. Lett. **86**, 082105 (2005).
[13]E. Rausch, B. Balke, S. Ouardi, and C. Felser, Phys. Chem. Chem. Phys. **16**, 25258 (2014).
[14]T. Wu, W. Jiang, X. Li, Y. Zhou, and L. D. Chen, J. Appl. Phys. **102**, 103705 (2007).
[15]S. R. Culp, J. W. Simonson, S. J. Poon, V. Ponnambalam, J. Edwards, and T. M. Tritt, Appl. Phys. Lett. **93**, 022105 (2008).
[16]X. Yan, G. Joshi, W. S. Liu, Y. C. Lan, H. Wang, S. Lee, J. W. Simonson, S. J. Poon, T. M. Tritt, G. Chen, and Z. F. Ren, Nano Lett. **11**, 556 (2011).
[17]S. Sumithra, N. J. Takas, D. K. Misra, W. M. Nolting, P. F. P. Poudeu, and K. L. Stokes, Adv. Energy Mater. **1**, 1141 (2011).
[18]K. F. Hsu, S. Loo, F. Guo, W. Chen, J. S. Dyck, C. Uher, T. Hogan, E. K. Polychroniadis, and M. G. Kanatzidis, Science **303**, 818 (2004).
[19]A. Bhardwaj and D. K. Misra, RSC Adv. **4**, 34552 (2014).
[20]G. J. Snyder, M. Christensen, E. Nishibori, T. Caillat, and B. B. Iversen, Nat. Mater. **3**, 458 (2004).
[21]A. Bhardwaj, A. Rajput, A. K. Shukla, J. J. Pulikkotil, A. K. Srivastava, A. Dhar, G. Gupta, S. Auluck, D. K. Misra, and R. C. Budhani, RSC Adv. **3**, 8504 (2013).
[22]L. D. Hicks and M. S. Dresselhaus, Phys. Rev. B **47**, 12727 (1993).
[23]G. J. Snyder and E. S. Toberer, Nat. Mater. **7**, 105 (2008).
[24]P. Sahoo, Y. Liu, J. P. A. Makongo, X. L. Su, S. J. Kim, N. Takas, H. Chi, C. Uher, X. Pana, and P. F. P. Poudeu, Nanoscale **5**, 9419 (2013).
[25]W. J. Xie, J. He, S. Zhu, X. L. Su, S. Y. Wang, T. Holgate, J. W. Graff, V. Ponnambalam, S. J. Poon, X. F. Tang, Q. J. Zhang, and T. M. Tritt, Acta Mater. **58**, 4705 (2010).
[26]Y. Liu, P. Sahoo, J. P. A. Makongo, X. Zhou, S. J. Kim, H. Chi, C. Uher, X. Pan, and P. F. P. Poudeu, J. Am. Chem. Soc. **135**, 7486 (2013).
[27]J. P. A. Makongo, D. K. Misra, X. Zhou, A. Pant, M. R. Shabetai, X. Su, C. Uher, K. L. Stokes, and P. F. P. Poudeu, J. Am. Chem. Soc. **133**, 18843 (2011).
[28]J. P. Makongo, D. K. Misra, J. R. Salvador, N. J. Takas, G. Wang, M. R. Shabetai, A. Pant, P. Paudel, C. Uher, K. L. Stokes, and P. F. P. Poudeu, J. Solid State Chem. **184**, 2948 (2011).
[29]J. E. Douglas, C. S. Birkel, M. S. Miao, C. J. Torbet, G. D. Stucky, T. S. Pollock, and R. Seshadri, Appl. Phys. Lett. **101**, 183902 (2012).
[30]R. A. Downie, D. A. MacLaren, and J.-W. G. Bos, J. Mater. Chem. A **2**, 6107 (2014).
[31]D. K. Misra, A. Bhardwaj, and S. Singh, J. Mater. Chem. **2**, 11913 (2014).
[32]Y. W. Chai and Y. Kimura, Appl. Phys. Lett. **100**, 033114 (2012).
[33]K. Kirievsky, Y. Gelbstein, and D. Fuks, J. Solid State Chem. **203**, 247 (2013).
[34]H. Kitagawa, M. Wakatsuki, H. Nagaoka, H. Noguchi, Y. Isoda, K. Hasezaki, and Y. J. Noda, Phys. Chem. Solids **66**, 1635 (2005).
[35]W. S. Liu, B. P. Zhang, J. F. Li, H. L. Zhang, and L. D. Zhao, J. Appl. Phys. **102**, 103717 (2007).
[36]S. V. Faleev and F. Leonard, Phys. Rev. B. **77**, 214304 (2008).
[37]J. M. O. Zide, J. H. Bahk, R. Singh, M. Zebarjadi, G. Zeng, K. Esfarjani, and A. Shakouri, J. Appl. Phys. **108**, 123702 (2010).
[38]J. L. Mi, X. B. Zhao, T. J. Zhu, and J. P. Tu, J. Phys. D: Appl. Phys. **41**, 205403 (2008).
[39]G. S. Nolas, J. Sharp, and H. J. Goldsmid, *Thermoelectric* (Springer, Berlin, 2001).
[40]G. S. Nolas, M. Kaeser, R. T. Littleton, and T. M. Tritt, Appl. Phys. Lett. **77**, 1855 (2000).
[41]See supplementary material at http://dx.doi.org/10.1063/1.4914504 for scanning electron microscopy (SEM) investigation.

This article is copyrighted as indicated in the article. Reuse of AIP content is subject to the terms at: http://scitation.aip.org/termsconditions. Downloaded to IP: 14.139.60.97 On: Tue, 20 Oct 2015 09:55:02